Mainstream Aerodynamic Effects Due to Wheelspace Coolant Injection in a High-Pressure Turbine Stage: Part II—Aerodynamic Measurements in the Rotational Frame

Christopher McLean[1]
e-mail: cmclean@techkor.com

Cengiz Camci
Professor of Aerospace Engineering
e-mail: cxc11@psu.edu

Turbomachinery Heat Transfer Laboratory,
The Pennsylvania State University,
University Park, PA 16802

Boris Glezer[2]
Consultant
San Diego, CA
e-mail: bglezer@san.rr.com

The current paper deals with the aerodynamic measurements in the rotational frame of reference of the Axial Flow Turbine Research Facility (AFTRF) at the Pennsylvania State University. Stationary frame measurements of "Mainstream Aerodynamic Effects Due to Wheelspace Coolant Injection in a High Pressure Turbine Stage" were presented in Part I of this paper. The relative aerodynamic effects associated with rotor–nozzle guide vane (NGV) gap coolant injections were investigated in the rotating frame. Three-dimensional velocity vectors including exit flow angles were measured at the rotor exit. This study quantifies the secondary effects of the coolant injection on the aerodynamic and performance character of the stage main stream flow for root injection, radial cooling, and impingement cooling. Current measurements show that even a small quantity (1 percent) of cooling air can have significant effects on the performance and exit conditions of the high-pressure turbine stage. Parameters such as the total pressure coefficient, wake width, and three-dimensional velocity field show significant local changes. It is clear that the cooling air disturbs the inlet end-wall boundary layer to the rotor and modifies secondary flow development thereby resulting in large changes in turbine exit conditions. Effects are the strongest from the hub to midspan. Negligible effect of the cooling flow can be seen in the tip region. [DOI: 10.1115/1.1397303]

Introduction

This publication continues the documentation of the effects of wheelspace coolant on the mainstream flow in the AFTRF high-pressure gas turbine stage. Part I of this paper entitled ''Mainstream Aerodynamic Effects Due to Wheelspace Coolant Injection in a High-pressure Turbine Stage: Part I—Stationary Frame Measurements,'' documented the effects of the wheelspace cooling air in the stationary measurement frame. Following the measurements and analysis of the stationary frame data, it was desired to observe the effects in the rotational frame of reference. Data measured in the rotational frame would contain circumferential variations due to the rotor. In the stationary frame these variations were averaged out. Only in the rotational frame could the rotor wake and three-dimensional rotor exit velocity field be observed.

Most turbine cooling research has been limited to cascade facilities simulating nozzle blades. Little documented research exists with aerodynamic measurements from spinning rotors with cooling flows. Cascade studies similar to those of Eckert [1], Friedrichs [2]. Jabbari [3,4], Goldstein [5], Gaugler [6] and Graziani [7] demonstrate the complex nature of endwall cooling with stationary blades. However, the spinning rotor complicates the mixing of the cooling flow with the mainstream flow. Centrifugal forces and the periodic nature of turbine aerothermodynamics Abhari [8] necessitate that cooling research be performed in rotational environments when rotors are concerned. Periodic effects such as the circumferential variation in turbine entry temperature (TET) and the time-dependent variation in mainstream flow caused by the blade rotation cause a wide variation in cooling effectiveness. The cooling effectiveness fluctuation is driven by a change in the time averaged mass flux exiting from the cooling holes and by the interaction of the coolant with the unsteady external flow. Coolant jets are shown to pulsate due to the fluctuations of the instantaneous static pressure at the jet exit. Variations in the instantaneous film cooling effectiveness can be as high as 230 percent (Abhari [8]). A full understanding of turbine cooling flow effects can only be realized through rotational frame measurements.

Experimental Test Facility

The Axial Flow Turbine Research Facility (AFTRF) (Fig. 1) is a cold open-loop facility 0.916 m in diameter with a single-stage, high-pressure, axial turbine blading configuration. The facility consists of a bellmouth inlet, a single high-pressure turbine stage with a nozzle guide vane (NGV) and rotor, and outlet guide vanes. Detailed stage characteristics of this turbine facility can be found in Lakshminarayana, et al. [9,10] and Zaccaria [11]. The facility was used for the current research program with modifications to allow for the wheelspace cooling. Some of the facility details are also provided in Part I of this paper. The AFTRF is unique in its ability to operate continuously with a traversable sensor package in the rotational frame of reference. The AFTRF is able to traverse five-hole, thermocouple, and hot-wire probes in the rotational frame. A full two-dimensional traverse system is incorporated into the wheelspace allowing probe movements in the r and Q direc-

[1]Present address: Division Manager, Techkor Instrumentation, A Division of ACT, Inc., Harrisburg, PA.

[2]Former Head of ''Turbine Cooling Design and Analysis'' at Solar Turbines Inc., San Diego, CA.

Contributed by the International Gas Turbine Institute and presented at the 46th International Gas Turbine and Aeroengine Congress and Exhibition, New Orleans, Louisiana, June 4–7, 2001. Manuscript received by the International Gas Turbine Institute February 2001. Paper No. 2001-GT-120. Review Chair: R. Natole.

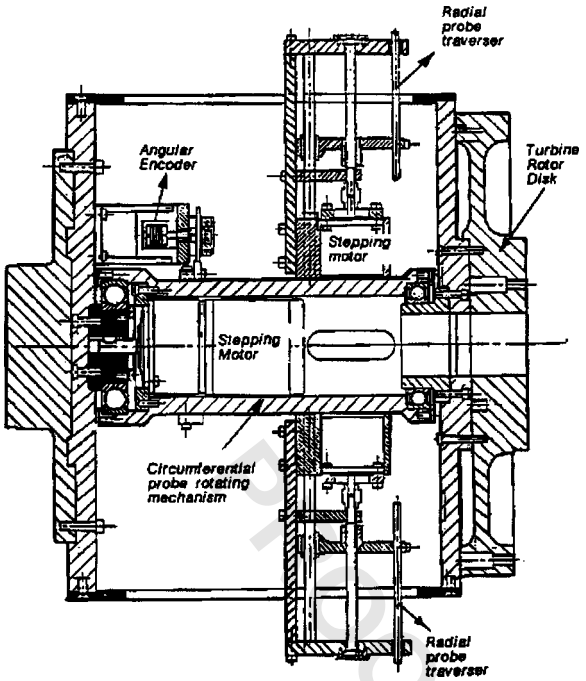

Fig. 1 Rotating instrument and traversing package contained within the rotor drum

Table 1 Coolant flow parameters for rotational frame measurements

Mass Flow Ratio $\dot{m}_C/\dot{m}_P$	Mean Discharge Velocity $U_C=\dot{m}_C/n\rho A$	Mean Discharge Mach Number $M=U_C/\sqrt{\gamma RT_C}$	Blowing Rate $\rho_C U_C/\rho_P U_P$	Velocity Ratio U_C/U_P
1.00%	158 m/s	0.46	1.56	3.95

tions over one rotor blade passage in the mainstream. A 150-channel slip ring passes measurement data from the rotational to stationary frame. The rotational frame data were taken with the same three configurations for cooling air injection as the stationary frame measurements. The geometry of the three cooling hole sets is shown in Part I of this publication.

The cooling flow parameters are summarized in Table 1 where the mass flow ratio was defined as $\dot{m}_C/\dot{m}_P$, the mean discharge velocity was defined as $U_C=\dot{m}_C/n\rho A$, the mean discharge Mach number was defined as $M=U_C/\sqrt{\gamma RT_C}$, the blowing rate was defined as $\rho_C U_C/\rho_P U_P$ and the velocity ratio was defined as U_C/U_P.

The scaling of the various cooling flow parameters was established by considering the operational conditions of modern turbines. Blowing rates available in the AFTRF agree well with those in the literature. All rotational frame data were taken with a mass flow ratio of 1 percent.

Measurements

Five-hole probe surveys in the AFTRF were taken with and without cooling injection in the rotational frame. The subminiature five-hole probe was installed 1.5 axial chords downstream of the rotor trailing edge, as shown in Fig. 2. Data were taken with the five-hole probe mounted in the rotational frame and traversed in the radial and circumferential directions ($r-\Theta$ traverse). Aerodynamic measurement details of this probe can be found in Wiedner [12]. The velocity data were normalized by U_m. The rotational traverse had a circumferential sweep of 1.10 rotor blade passages.

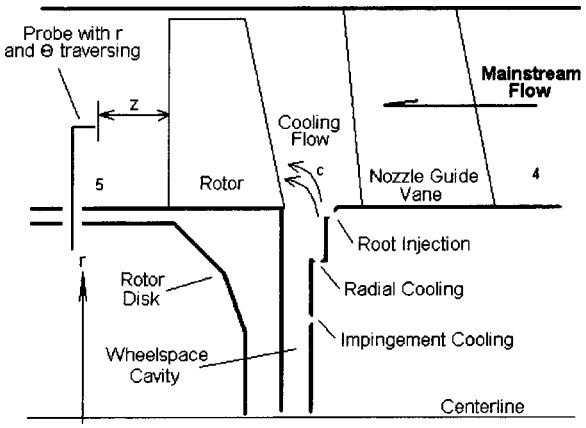

Fig. 2 Schematic diagram showing the placement of the five-hole probes for rotational frame data

The cooled and noncooled data were taken in an interlaced manner. At each measurement point in the traverse grid, the probe readings were recorded with and without cooling flow. A set of high-speed solenoids controlled the coolant flow. This method ensured that the cooled and noncooled cases experienced the same mainstream flow conditions. Small variations in mainstream flow would otherwise be misreported as changes due to the cooling flow.

The three-dimensional velocity field was measured with a subminiature five-hole probe. A data reduction method explained in Brophy et al. [13] was implemented. Measurement corrections due to the rotation of the probe mounted to the rotor exit were performed during the data reduction. The signals from the pressure transducers were internally amplified and passed through the slip ring to the stationary frame. The signals were then sampled via a personal computer with an analog to digital converter. Cooled and noncooled data ($P'_{05.1}, P'_{05.2}, P'_{05.3}, P'_{05.4}, P'_{05.5}$) were sampled at 100 Hz for 15 seconds at each measurement point. The measured data at this sampling rate and duration was statistically stable. The resulting data were statistically averaged and proper calibration equations were applied. The result were data sets for cooled and noncooled cases containing P_O, P_S, u, v, w, U, α, and β in the rotational frame. The legend for the data is given in Fig. 3.

Total Pressure Coefficient. The total pressure coefficient in the rotational frame was

$$\tilde{C}_p=\frac{\tilde{P}_{05}}{1/2\rho U_m^2} \tag{1}$$

computed from the following equation where the total pressure was measured with the rotating five-hole probe. The rotational total pressure was defined as:

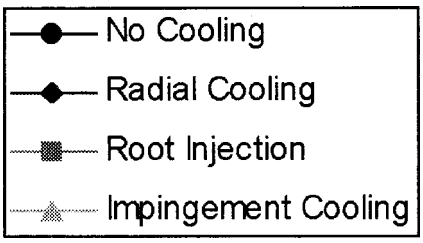

Fig. 3 Legend for data presentation of coolant flow measurements

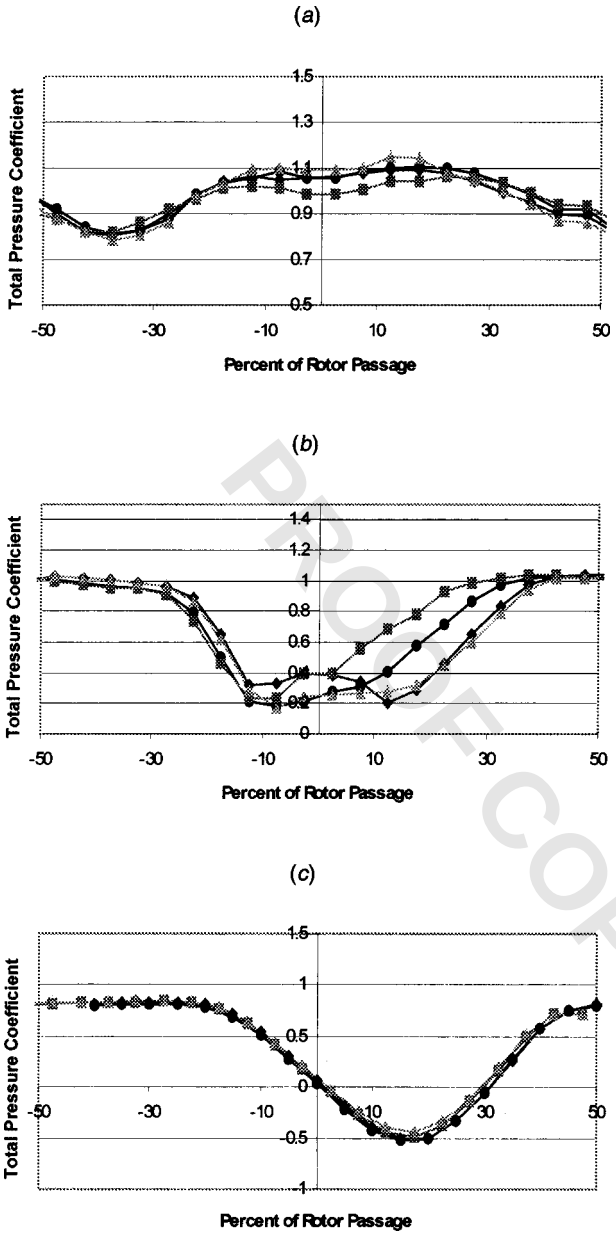

Fig. 4 Total pressure loss coefficient in rotational frame at *H* of 0.15 (*a*), 0.50 (*b*), and 0.90 (*c*). Probe 1.5 chords downstream of the rotor exit.

$$\tilde{P}_{05} = \tilde{P}_5 + \frac{1}{2}\rho\tilde{U}^2 \tag{2}$$

The total pressure coefficient, shown in Fig. 4, displays the rotor wake at three sections: hub ($H = 0.15$), midspan ($H = 0.50$), and tip ($H = 0.90$).

At the hub section ($H = 0.15$), the effects of the cooling injection are minimal. The radial and impingement cooling show relatively small changes of 3 percent. With the root injection, the magnitude of the wake is changed by up to 8 percent. It should be noted that the changes of root injection are opposite in direction to those of radial and impingement cooling.

The total pressure coefficient at the midspan ($H = 0.50$) shows significant effects due to cooling injection. The 1 percent cooling injection has the ability to produce up to 88 percent local changes in total pressure coefficient (midspan, root injection, center of wake). The root injection reduces the width of the wake region while the radial, and impingement cooling causes the wake width to increase. The large changes in the rotor wake are due to a shift in the wake position and wake width rather than a change in the wake peak or trough magnitudes. For this reason the total pressure coefficient in the stationary frame (loss coefficient) shows relatively small changes (1 to 3 percent) due to cooling (see Fig. 7 in Part I of this publication). The changes observed in the stationary frame are due to a change in the rotor wake width in the rotational frame. The effect of the width change is smoothed out in the stationary frame measurements. To understand the physical mechanism, responsible for the loss coefficient changes it is necessary to look in the rotational frame.

At the tip section ($H = 0.90$), the effects of the cooling injection are immeasurable. The cooling air does not mix with or effect the tip flow region. The variations found in the pressure loss data are similar to that found by Friedrichs [14] in an endwall cooling study. He states that the change in overall loss is small for endwall cooling and can be positive or negative depending on the coolant supply pressure. The direction of change would also depend on the cooling geometry.

Velocity Components. Axial, tangential, and radial velocity data are shown in Figs. 5, 6, and 7. All data have been normalized by the blade rotational velocity at midspan (U_m) as shown in Eqs. (3)–(5):

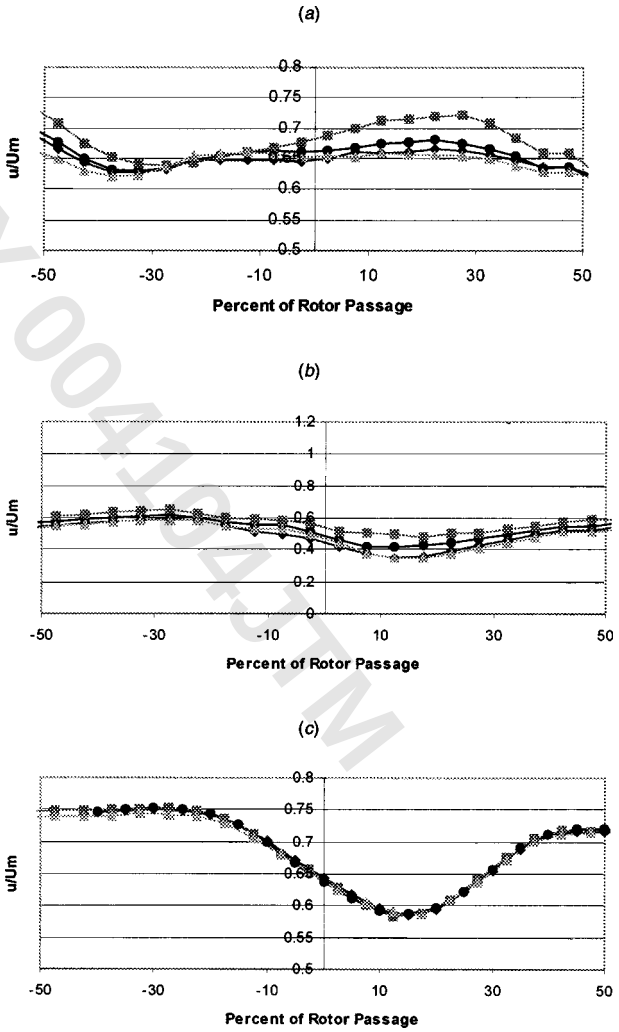

Fig. 5 Axial velocity in the rotational frame at *H* of 0.15 (*a*), 0.50 (*b*), and 0.90 (*c*). Probe 1.5 chords downstream of the rotor exit.

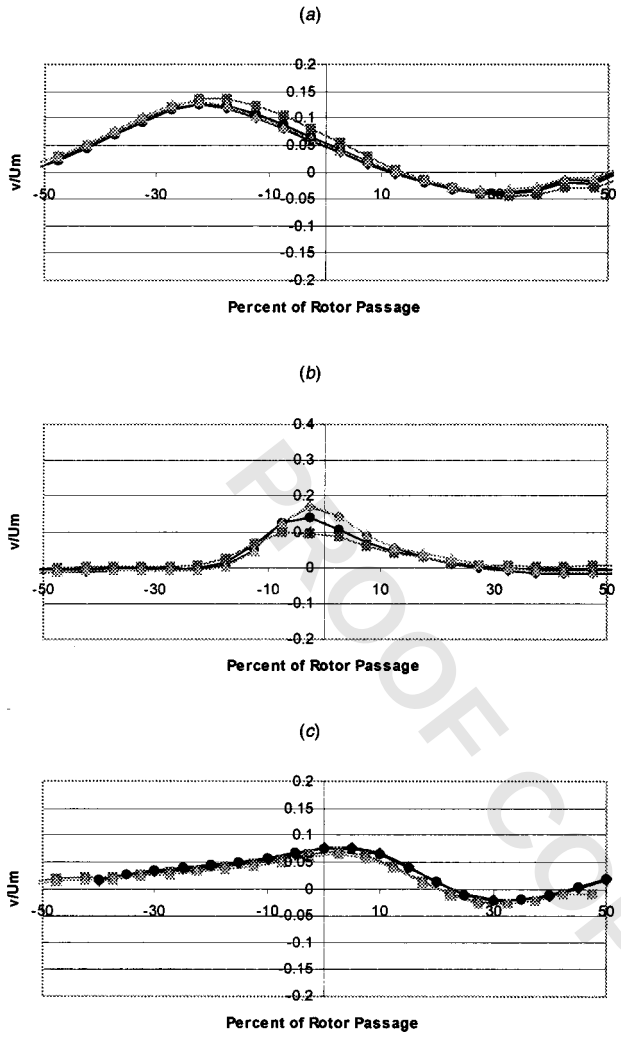

Fig. 6 Radial velocity in the rotational frame at *H* of 0.15 (*a*), 0.50 (*b*), and 0.90 (*c*). Probe 1.5 chords downstream of the rotor exit.

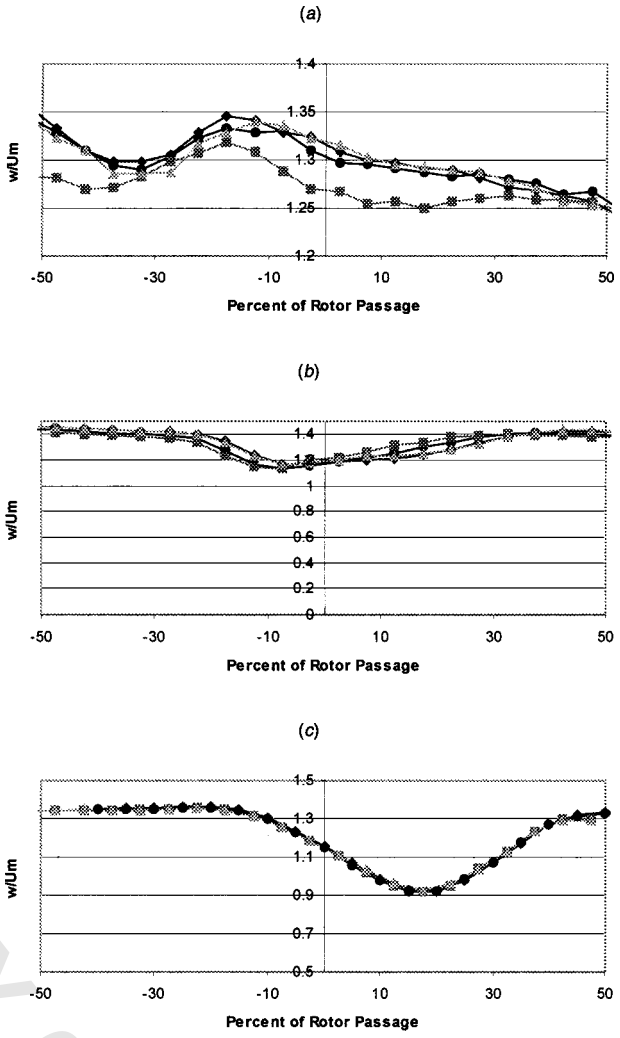

Fig. 7 Tangential velocity in the rotational frame at *H* of 0.15 (*a*), 0.50 (*b*), and 0.90 (*c*). Probe 1.5 chords downstream of the rotor exit.

$$\tilde{u}_{\text{normalized}} = \frac{u}{U_m} \tag{3}$$

$$\tilde{v}_{\text{normalized}} = \frac{\tilde{v}}{U_m} \tag{4}$$

$$\tilde{w}_{\text{normalized}} = \frac{\tilde{w}}{U_m} \tag{5}$$

The axial velocity (u) shows significant changes at the hub ($H = 0.15$) and midspan ($H = 0.50$) locations. At both the hub and midspan locations, the root injection tends to increase the axial velocity and the radial and impingement cooling tend to decrease the axial velocity. At the hub, the magnitudes of the root injection are twice those of the radial and impingement cooling. At the midspan, the magnitudes are comparable.

The axial velocity has immeasurable changes at the tip ($h/H = 0.90$). As was observed in the pressure coefficient data, the cooling flow does not mix with or affect the tip flow region. The tangential velocity (w) shows significant effects due to the cooling flow at the hub ($H = 0.15$) and midspan ($H = 0.50$) locations. The effect is reversed from that seen in the axial velocity. At both the hub and midspan locations, the root injection tends to decrease the axial velocity and the radial and impingement cooling tend to increase the axial velocity. At the hub, the magnitudes of the root injection changes (3.5 percent) are considerably higher than those of the radial and impingement cooling (0.5 percent). At the midspan, the magnitudes are comparable (4 percent). The tangential velocity has immeasurable changes at the tip ($H = 0.90$). As was observed in the pressure coefficient data, the cooling flow does not mix with or affect the tip flow region.

The radial velocities in the AFTRF tend to be small in magnitude, but large changes were observed in their magnitudes. The largest changes were observed at the midspan. Root injection was able to decrease the radial velocity by as much as 30 percent, while the radial and impingement cooling were able to decrease the axial velocity by up to 20 percent.

The radial velocity has immeasurable changes at the tip ($H = 0.90$). As was observed in the pressure coefficient data, the cooling flow does not mix with or affect the tip flow region.

Exit Angles. With the three-dimensional velocity field known, it was possible to compute the exit angles for the turbine stage. The exit angle in the axial-tangential plane (β) is shown in Fig. 8 and the exit angle in the axial-radial plane (α) is shown in Fig. 9. The axial–radial plane (α) exit angle shows significant variation at the hub ($H = 0.15$) and midspan ($H = 0.50$) sections. The change is driven by the large magnitude changes in the radial velocity. At the hub, the root injection increased the exit angle by up to 2 deg. At the midspan, the root injection decreases the exit

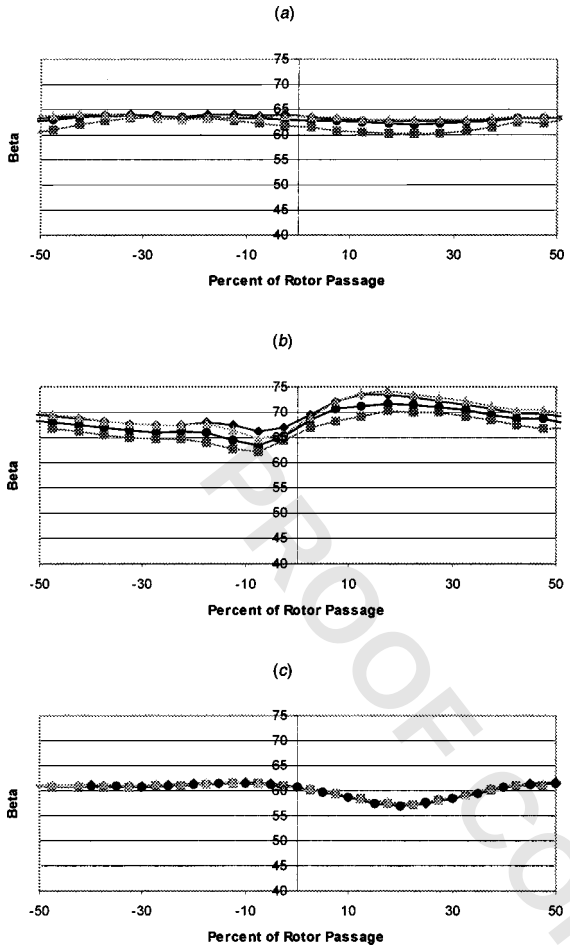

Fig. 8 Exit angle in the rotational axial-tangential plane (β) at H of 0.15 (*a*), 0.50 (*b*), and 0.90 (*c*). Probe 1.5 chords downstream of the rotor exit.

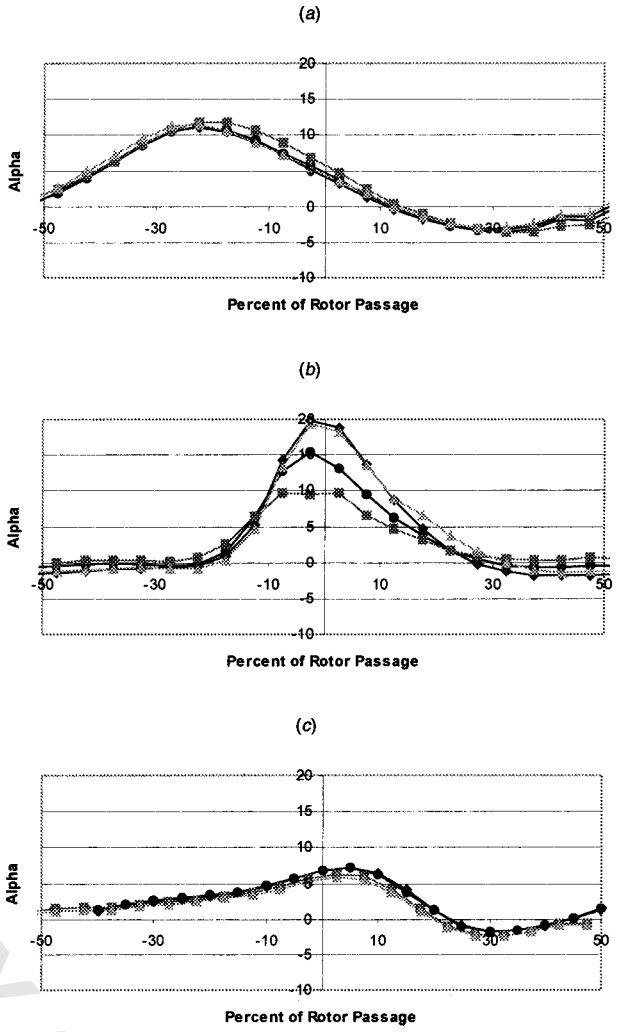

Fig. 9 Exit angle in the rotational axial-radial plane (α) at H of 0.15 (*a*), 0.50 (*b*), and 0.90 (*c*). Probe 1.5 chords downstream of the rotor exit.

angle by up to 5 deg, while the radial and impingement cooling increase the exit angle by up to 5 deg. At the tip region, root injection and impingement cooling were able to reduce the exit angle by 1 deg while radial cooling had no effect.

The axial–tangential plane (β) exit angle shows significant variation at the hub ($H=0.15$) and midspan ($H=0.50$) sections. The variations follow the changes in velocity in the axial and tangential directions. At the hub the root injection reduces the exit angle by up to 2.5 deg. The radial and impingement cooling show little effect. At the midspan location, the root injection reduces the exit angle by up to 2.5 deg while the radial and impingement cooling increase the exit angle by up to 2.5 deg. At the tip region none of the cooling flows show any measurable changes.

The opposite changes found in the rotational frame measurements are consistent with the exit angle changes seen in the stationary frame. However, in the stationary frame it was found that the radial and impingement exit angle changes were caused by a radial outward shift in the profiles, not a change in their overall magnitudes.

This would seem to indicate that the passage vortex location is being modified but that the strength is not. Friedrichs et al. [2] also observed that endwall platform cooling could significantly shift the location of the passage vortex but that the strength was not significantly affected.

Conversely, root injection in the stationary frame was found to be able to reduce the magnitude of the passage vortexes, thereby changing the overall magnitude of the exit angle. Friedrichs et al. [14] also observed that significant cooling injection could delay the three-dimensional separation of the inlet boundary layer thereby reducing the strength of the passage vortex.

Time Accurate Dynamic Pressure. Measurements of the surface pressure on the leading edge of the rotor were performed ($H=0.10$). The AFTRF contained embedded Kulite pressure transducers with a very high dynamic response. The Kulite transducers had thermal and long-term stability problems that prevented them from being calibrated for absolute pressure measurements. However, the Kulites were useful in measuring the relative changes in the nozzle wakes. The response time of the Kulites was fast enough to capture individual nozzle wakes as seen from the rotor tip.

A comparison of the three baseline measurements was performed to determine the level of repeatability in the Kulite data. Excellent repeatability was found between the three runs. Ensemble-averaged dynamic pressure data are shown in Fig. 10 for root injection. The 23 individual nozzle blade passings are visible in the measurement data. It should be noted that slight differences exist between the wakes. Each nozzle has a distinct wake profile. When taking data in the rotational frame only one specific wake profile is being analyzed, while when taking data in the stationary frame all wakes are being measured and averaged by the probe. As a result, comparisons between rotational frame data and stationary frame data must be made carefully.

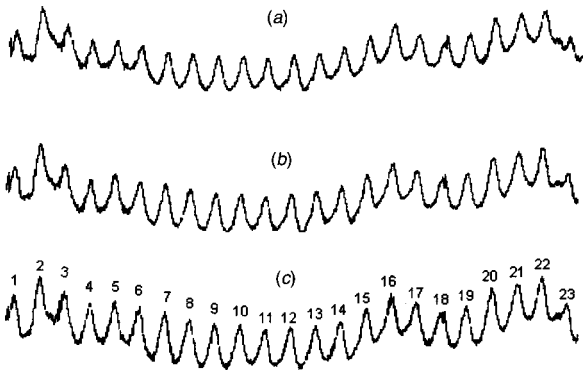

Fig. 10 Pressure measurements on the rotor leading edge for root injection blowing ratios of 1.00 percent (*a*), 1.25 percent (*b*), and 1.50 percent (*c*)

Fig. 11 Kulite data from the rotor platform. The root injection (jagged line) shows noticeable wake reduction from the non-cooled case. Four vane passages are shown.

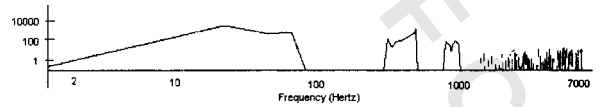

Fig. 12 Frequency domain processing of leading edge Kulite run data with fast Fourier transform

The frequency domain processed data are shown in Figs. 11 and 12. Several fundamental frequency components can be seen including the once-per-rev (22 Hz), nozzle blade passing (507 Hz), and twice nozzle blade passing (1014 Hz).

Conclusions

The effects of small (1 percent) coolant injection into the free stream of a high-pressure turbine stage can be very significant and should not be neglected on the aerodynamic analysis of turbine stages. The cooling air is affecting the structure of the three-dimensional secondary flow and inlet rotor boundary layer, which in turn has a large effect on the exit three-dimensional flow and stage performance.

The changes observed were large and three-dimensional in nature. Their neglect in stage blading design could lead to serious miscalculations. Parameters such as pressure coefficient, wake width, three-dimensional velocity field, and exit angles were observed to change significantly.

The cooling was able to produce significant changes in the total pressure coefficient. The large changes in pressure coefficient are due to a shift in the wake position and wake width rather than a change in the wake peak or trough magnitudes. In the rotational frame, root injection reduced the width of the wake while radial and impingement cooling increased the width. The effects of the rotational frame width changes are smoothed out in the stationary frame measurements. To understand the physical mechanism responsible for the loss coefficient changes (stationary frame), it is necessary to look in the rotational frame.

Root injection tended to have an opposite effect on the three-dimensional velocity field from radial and impingement cooling. This is consistent with the stationary frame data provided in Part I of this publication. Again, it is necessary to examine both the stationary and rotational frames to have a complete understanding of the physics controlling the velocity field.

The changes in rotor exit flow are highest at the midspan. The effects of the cooling are convected to the midspan by the action of the passage vortices. It is believed that the cooling air is energizing the boundary layer ahead of the rotor thereby effecting the development and effects of the secondary flows.

Additional research should be performed to detail the complex cooling-mainstream mixing process and its effects on the inlet rotor boundary layer and the resulting secondary flows.

Acknowledgments

This paper is based on university research funded by the U.S. Dept. of Energy, AGTSR program. The authors would like to acknowledge Drs. L. Golan, D. Fant, and R. Wenglarz as program monitors.

Nomenclature

A = exit area of single cooling hole
b = $\rho_C U_C / \rho_P U_P$
H = normalized radial position$=(r-r_h)/L$
h = entropy
L = rotor blade height
M = Mach number
$\dot{m}$ = mass flow rate
n = number of cooling holes (23)
P = pressure
R = gas constant
r = radial position
T = temperature
U, V, W = wheel speed, relative, velocity, absolute velocity
u = axial velocity component
v = radial velocity component
w = tangential velocity component
α = pitch angle, exit flow angle inclined to the turbine axis
β = yaw angle, exit flow angle
γ = ratio of specific heats
Θ = angle in circumferential direction
ρ = density

Subscripts

c = cooling
o = total condition
04 = entry of nozzle condition
05 = exit of rotor condition
h = hub
m = blade rotational velocity at midspan
p = primary
s = static condition
total = total condition

Superscripts

~ = rotational frame value

References

[1] Eckert, E., 1984, ''Analysis of Film Cooling and Full Coverage Film Cooling of Gas Turbine Blades,'' ASME J. Eng. Gas Turbines Power, **106**, pp. ■■.
[2] Friedrichs, S., Hodson, H., and Dawes, W., 1997, ''Aerodynamic Aspects of Endwall Film-Cooling,'' ASME J. Turbomach., **119**, pp. 786–793.
[3] Jabbari, M., and Goldstein, R., 1993, ''Film Cooling, Mass Transfer, and Flow at the Base of a Turbine Blade,'' J. Eng. Phys. Thermophys., **65**, No. 3, pp. ■■.
[4] Jabbari, M., Marston, K., Eckert, E., and Goldstein, R., 1996, ''Film Cooling of the Gas Turbine Endwall by Discrete-Hole Injection,'' ASME J. Turbomach., **118**, pp. 278–284.
[5] Goldstein, R., and Chen, H., 1985, ''Film Cooling on a Gas Turbine Blade Near the End Wall,'' ASME J. Eng. Gas Turbines Power, **107**, pp. ■■.
[6] Gaugler, R., and Russell, L., 1984, ''Comparison of Visualized Turbine Sec-

ondary Flows and Measured Heat Transfer Patterns,'' ASME J. Eng. Gas Turbines Power, **106**, pp. ■■.
[7] Graziani, R., Blair, M., Taylor, J., and Mayle, R., 1980, ''An Experimental Study of Endwall and Airfoil Surface Heat Transfer in a Large Scale Turbine Blade Cascade,'' ASME J. Eng. Power, **102**, pp. 257–267.
[8] Abhari, R., 1996, ''Impact or Rotor-Stator Interaction on Turbine Blade Film Cooling,'' ASME J. Turbomach., **118**, pp. ■■.
[9] Lakshminarayana, B., Camci, C., Halliwell, I., and Zaccaria, M., 1992, ''Investigation of Three Dimensional Flow Field in a Turbine Including Rotor/Stator Interaction,'' presented at the AIAA/SAE/ASME/ASEE 28th Joint Propulsion Conference and Exhibit, July 6–8, Nashville, TN.
[10] Lakshminarayana, B., Camci, C., Halliwell, I., and Zaccaria, M., 1996, ''Design and Development of a Turbine Research Facility to Study Rotor-Stator Interaction,'' Int. J. Turbo and Jet Engines, **13**, pp. 155–172.
[11] Zaccaria, M. A., 1994, ''Investigation of Three Dimensional Flow Field in a Turbine Including Rotor/Stator Interaction,'' Ph.D. Thesis in Aerospace Engineering, The Pennsylvania State University.
[12] Wiedner, G., 1994, ''Passage Flow Structure and its Influence on Endwall Heat Transfer in a 90° Turning Duct,'' Ph.D. Thesis in Aerospace Engineering, The Pennsylvania State University.
[13] Brophy, M., Treaster, A., Stinebring, D., and Welz, J., 1984, ''Optimization of a Five-Hole Probe Wake Measurement System,'' Applied Research Laboratory, The Pennsylvania State University.
[14] Friedrichs, S., Hodson, H. P., and Dawes, W. N., 1995, ''Distribution of Film-Cooling Effectiveness on a Turbine Endwall Measured Using the Ammonia and Diazo Technique,'' ASME Paper No. 95-GT-1.